Physics of Fluids

Linear stability analysis of one-dimensional detonation coupled with vibrational relaxation

Cite as: Phys. Fluids **32**, 126101 (2020); https://doi.org/10.1063/5.0029468
Submitted: 16 September 2020 • Accepted: 04 November 2020 • Published Online: 01 December 2020

Ken Chun Kit Uy (黃駿傑), Lisong Shi (时立松), Jiaao Hao (郝佳傲), et al.

View Online Export Citation CrossMark

ARTICLES YOU MAY BE INTERESTED IN

The influence of the equation of state on the cellular structure of gaseous detonations
Physics of Fluids **33**, 036105 (2021); https://doi.org/10.1063/5.0040723

Computational study of gaseous cellular detonation diffraction and re-initiation by small obstacle induced perturbations
Physics of Fluids **33**, 047115 (2021); https://doi.org/10.1063/5.0044164

A computational study of the interaction of gaseous detonations with a compressible layer
Physics of Fluids **29**, 056101 (2017); https://doi.org/10.1063/1.4982659

AIP Publishing

© 2020 Author(s).

Physics of Fluids ARTICLE scitation.org/journal/phf

Linear stability analysis of one-dimensional detonation coupled with vibrational relaxation

Cite as: Phys. Fluids 32, 126101 (2020); doi: 10.1063/5.0029468
Submitted: 16 September 2020 • Accepted: 4 November 2020 •
Published Online: 1 December 2020

View Online Export Citation CrossMark

Ken Chun Kit Uy (黃駿傑),[a] Lisong Shi (时立松),[b] Jiaao Hao (郝佳傲),[c] and Chih-Yung Wen (温志湧)[d]

AFFILIATIONS

Department of Mechanical Engineering and Interdisciplinary Division of Aeronautical and Aviation Engineering, The Hong Kong Polytechnic University, Hung Hom, Kowloon, Hong Kong

[a]Email: 16901590r@connect.polyu.hk
[b]Email: lisong.shi@connect.polyu.hk
[c]Email: jiaao.hao@polyu.edu.hk
[d]Author to whom correspondence should be addressed: cywen@polyu.edu.hk

ABSTRACT

The linear stability of one-dimensional detonations with one-reaction chemistry coupled with molecular vibration nonequilibrium is investigated using the normal mode approach. The chemical kinetics in the Arrhenius form depend on an averaged temperature model that consists of translational–rotational mode and vibrational mode. The Landau–Teller model is applied to specify the vibrational relaxation. A time ratio is introduced to denote the ratio between the chemical time scale and the vibrational time scale in this study, which governs the vibrational relaxation rate in this coupling kinetics. The stability spectrum of disturbance eigenmodes is obtained by varying the bifurcation parameters independently at a different time ratio. These parameters include the activation energy, the degree of overdrive, the characteristic vibrational temperature, and the heat release. The results indicate that the neutral stability limit shifts to higher activation energy on the vibrational nonequilibrium side with a smaller time ratio, implying that the detonation is stabilized. A similar observation is seen at a lower degree of overdrive. Compared with the above two parameters, the characteristic vibrational temperature plays a minor role in the stabilization of detonation, and no change in the number of eigenmodes is identified throughout the selected range. By plotting the neutral stability curves relating the heat release to the above parameters, the decreases in instability ranges are obviously seen under vibrational nonequilibrium. The thermal nonequilibrium effect on detonation stability is clearly demonstrated. The analysis presented in this paper is ultimately justified by comparing the results with numerical simulation.

Published under license by AIP Publishing. https://doi.org/10.1063/5.0029468

I. INTRODUCTION

Detonation is a shock-induced supersonic wave in which the reactants are ignited and burned such that the energy released from the chemical reaction helps in sustaining self-propagation. A well-known one-dimensional steady-state solution to describe such a process is the Zel'dovich–von Neumann–Döring (ZND) model developed in the mid-20th century[1–3] in which the detonation structure is manifested by a single-step Arrhenius equation. A detonation with the minimum self-propagation speed is known as the Chapman–Jouguet (CJ) detonation, where an equilibrium sonic flow can be found at the end of the reaction zone. However, detonation waves in experiments often show a cell or diamond structure if propagating in a rectangular channel, which is attributed to cellular instability.[4] Due to the multi-dimensional nature of the flow, triple points are formed by the interaction of the incident shock and the Mach stem in which the shock propagates transverse and is reflected between the collisions. The importance of understanding the stability behavior of a detonation wave is thus addressed. These studies are crucial in many engineering applications involving the transfer rate of energy in a detonation, particularly in the design of an oblique detonation engine[5–7] and rotating detonation engine.[8] An overview of the detonation stability theory on the application in propulsion can be found in the work of Stewart and Kasimov.[9]

The works on detonation stability theory began in the 1960s, when Erpenbeck developed a linear stability analysis (LSA) to investigate the stability behavior of an idealized detonation. With the

Laplace transform approach discussed in his work,[10–12] the overall linear stability of a detonation is first demonstrated mathematically by analyzing the governing equations with perturbation involved in the problem. The neutral stability boundary is provided in these studies, but information regarding the number of unstable modes and the growth rates and frequencies of the most unstable modes are not provided in detail. Later, a normal mode approach was developed to address the same problem[13] in which the authors utilized a numerical shooting algorithm under the acoustic boundary condition at the end of the reaction. Through this algorithm, growth rates and frequencies of the unstable modes and the corresponding neutral stability limit denoted by the zero growth rate have been determined by solving the eigenvalues. The parametric study was also conducted by varying different parameters (i.e., change in activation energy and that in the degree of overdrive). Following the work of Lee and Stewart,[13] Sharpe[14] derived a similar approach based on the normal mode analysis, and an asymptotic solution of the ordinary differential equations for the linear perturbations was revealed. Using their work on idealized detonation as the basis, LSA in other forms of detonation was then being investigated; for instance, the dynamics of the initial cellular detonation formation process,[15] pathological detonation,[16] spinning detonation,[17] and curved detonation.[18] Notably, LSA cannot predict the perturbation structure far from the stability limit, since the detonation at this condition is very nonlinear and the prediction of bifurcations to multi-mode and irregular oscillations becomes unfavourable.[19] An example of a mismatch in the detonability limit between the numerical calculation and LSA using a chain-branching reaction model was reported by Short and Quirk.[20] However, LSA remains a powerful tool to study the detonation stability as the first step because this method gives an excellent estimation of the neutral stability values and frequencies near the stability limit without excessive computational cost. LSA can serve as the benchmark for validation of tested cases.[16]

With the increase in computation power in recent decades, the study of detonation stability has been extended from pure mathematical analysis to the numerical integration of time-dependent reactive Euler equations because the nonlinearity of the problem can be fully retained in the simulation. In addition, multi-dimensional stability can be investigated separately during the interpretation of the numerical results.[21] However, simulating the case near the stability limit may take a long time because the growth or decay rate of the perturbation is slow. Very fine numerical temporal and spatial resolutions may be required during numerical integration, which can be formidable. Nevertheless, numerical simulation has been adopted by many researchers to study different detonation problems with reaction chemistry involving chain-branching kinetics[22,23] and pulsating detonation.[19,24] As mentioned before, both the analysis from the normal mode approach and that from numerical integration should show be in fair agreement near the stability limit, which is relatively linear in nature. Analytical studies (through LSA) and numerical simulations of the detonation stability problem are therefore commonly conducted at the same time so that the results from different approaches can be compared for validation.[25–28]

Concurrently, the modeling of detonation chemistry has been kept updated by researchers to imitate the actual chemical kinetics occurring in experiments. The study of Taylor *et al.*[29] on the determination of ignition time scale and vibrational time scale in a stoichiometric H_2/air detonation revealed that the vibrational relaxation mechanism does not need to be at an equilibrium state right after the onset of the reaction because the two time scales could be comparable with each other. For instance, the ratio of the ignition delay time over the vibrational relaxation time is less than 3 for H_2 under the post-shock state of a Chapman–Jouguet detonation (i.e., at 28 atm and 1540 K) with the stoichiometric H_2–air mixture at 1 atm and 300 K initially. Under this background, Shi *et al.*[30] simulated both one-dimensional and two-dimensional H_2/O_2 detonation diluted with argon at vibrational equilibrium and nonequilibrium, respectively. They found that both the half-reaction length and the computed detonation cell size are enlarged if vibrational relaxation is considered, and the comparable cell size with experiments indicates that this relaxation mechanism should be included in future studies related to gaseous detonation. In addition, the significance of vibrational relaxation in flame ignition and supersonic scramjet combustion has also been reported recently in the literature.[31–33] From a theoretical perspective, Uy *et al.*[34,35] proposed an extended ZND model with a vibrational relaxation mechanism introduced in the one-step chemical kinetics, denoted as the chemical–vibrational coupling mechanism. They revealed that the energy transfer between the translational–rotational mode and the vibrational mode indeed reduced the overall chemical reaction rate, leading to an enlargement of the half-reaction length computed under the vibrational nonequilibrium assumption. A critical time ratio $\tau^{c/v}$ defined as the chemical reaction time scale τ_c vs vibrational relaxation time scale τ_v was introduced in their work, below which vibrational nonequilibrium should be considered in the analysis.

Referring to the works discussed above on the effect of different chemical kinetics in detonation stability analysis, it is interesting to know if the proposed chemical–vibrational coupling mechanism in gaseous detonation would also play a role in stabilizing the detonation propagation. In particular, a shift of the neutral stability boundary is expected because the overall chemical reaction rate will be changed at different states of vibrational nonequilibrium. This work will mainly adopt LSA to analytically determine the unstable mode of the related detonation near the stability limit. Note that due to the nonlinearity in the real reactive flow systems, the related stability analysis is suggested to be conducted further using numerical simulation with detailed chemistry, which will be studied in the future. For reference, Han *et al.*[36] have utilized a similar approach in the investigation of one-dimensional detonation stability under different Ar dilution in the H_2–O_2 mixture.

This paper has three objectives. First, the governing equations of the detonation, including the vibrational relaxation model, are presented, and the steady one-dimensional solutions of these equations are considered. The linearized equations are then determined with the introduction of small perturbations. A comparison of the normal mode result at the equilibrium state with that found in the literature is demonstrated for validation. Second, the normal mode linear stability spectra at different states of nonequilibrium denoted by $\tau^{c/v}$ are presented by varying four parameters: the activation energy in the chemical model, the degree of overdrive, the characteristic vibrational temperature, and the heat release in the relaxation model. The unstable mode and the stability limit for each state are identified. Finally, the governing equations are solved numerically

Published under license by AIP Publishing

such that the results can be compared with those from LSA. Justifications of using both analytical and numerical approaches to study detonation stability with vibrational–chemical coupling kinetics are provided, and a critical $\tau^{c/v}$ under which vibrational relaxation becomes significant is suggested.

II. GOVERNING EQUATIONS

In this section, the formulation of reactive Euler equations in the normalized one-dimensional forms with the inclusion of the vibrational relaxation mechanism in the single-step Arrhenius model is presented first. Then, the steady-state solution is obtained accordingly in Subsection II B and served as the input of the linear stability analysis discussed in Subsection II C.

A. Single-step Arrhenius kinetics with vibrational relaxation

The governing equations to describe a reaction flow inside a channel are given as

$$\frac{Dv}{Dt} - v\nabla \cdot u^l = 0, \frac{Du^l}{Dt} + v\nabla \cdot p = 0, \frac{De}{Dt} + p\frac{Dv}{Dt} = 0, \tag{1}$$

where v, u, p, and e are the specific volume (i.e., reciprocal of the density ρ), the fluid velocity, the pressure, and the specific internal energy, respectively. Superscript l denotes the coordinate system in the laboratory frame reference. The material derivative is written as

$$\frac{\mathrm{D}}{\mathrm{D}t} = \frac{\partial}{\partial t^l} + u^l\frac{\partial}{\partial x^l},$$

which is one-dimensional with a single velocity component u^l only. The corresponding internal energy with vibrational energy included to manifest the vibrational nonequilibrium effect is expressed as follows (in nondimensional form):

$$e = \frac{pv}{\gamma - 1} - \lambda\beta + \varepsilon, T_{\mathrm{tr}} = pv, \tag{2}$$

$$\varepsilon = \frac{\eta}{\exp(\eta/T_{\mathrm{v}}) - 1}, \tag{3}$$

where γ, λ, β, ε, η, T_{tr}, and T_{v} denote the specific heat ratio, reaction progress variable for the product, heat release, specific vibrational energy, characteristic vibrational temperature, translational–rotational temperature, and vibrational temperature, respectively. To facilitate the analysis of the vibrational–chemical coupling effect on the detonation stability, the specific internal energy is separated into three parts in Eq. (2), i.e., the translational–rotational mode of energy [the first term on the right-hand side of Eq. (2)], the heat addition per unit mass due to the chemical reaction (the second term), and the specific vibrational energy (the third term).

The translational–rotational mode of energy is assumed to be in equilibrium immediately after the shock, while the vibrational mode of energy still undergoes a significant relaxation. The translational–rotational temperature T_{tr} is correlated with pressure and specific volume by the equation of state. The specific vibrational energy is expressed as a function of the characteristic vibrational temperature η and corresponding vibrational temperature T_{v}, which follows the literature from statistical thermodynamics.[37] To facilitate a simple theoretical analysis, it is assumed that the reactant and product share the same characteristic vibrational temperature to evaluate the vibrational energy. Taking stochiometric combustion of a hydrogen and oxygen mixture as an example, H_2 (dimensional characteristic vibrational temperature $\bar{\phi}$ = 5989 K) only makes up a small portion of the overall vibrational energy due to its much lower mass fraction and larger $\bar{\phi}$ compared to O_2 ($\bar{\phi}$ = 2250 K). As the product, H_2O is a nonlinear triatomic molecule with three nondegenerate modes of vibration, including the symmetric stretching ($\bar{\phi}$ = 5266 K), antisymmetric deformation ($\bar{\phi}$ = 2297 K), and antisymmetric stretching ($\bar{\phi}$ = 5409 K) modes, of which the antisymmetric deformation mode contributes most to the vibrational energy due to the fact that the maximum detonation temperature is commonly about 3000 K. Therefore, it is reasonable to assume a single $\bar{\phi}$ (or η) for both the reactant and product to simplify the analysis. The effect of various species on detonation stability will be addressed in a future study by using direct numerical simulations with detailed mechanisms.

To describe a chemical reaction within the reaction zone, $\lambda = 0$ indicates the unburned reactant state, whereas $\lambda = 1$ represents the completion of the reaction. The normalized chemical reaction rate can then be modeled by a single-step Arrhenius equation and is given as

$$\frac{D\lambda}{Dt} = r = K(1-\lambda)\exp\left(-\frac{\vartheta}{T_{avg}}\right), \tag{4}$$

$$T_{avg} = \sqrt{T_{\mathrm{tr}}T_{\mathrm{v}}}, \tag{5}$$

where ϑ is the activation energy and K is the pre-exponential factor for the reaction. Together with Park's two-temperature model[38] expressed in Eq. (5) in which T_{avg} is the averaged temperature of T_{tr} and T_{v}, the vibrational–chemical coupling kinetics can be manifested in the simplest manner for analysis. Comparison with recent quasi-classical trajectory calculations of key hydrogen–air combustion reactions revealed that Parks' model can underestimate the reaction rate constants under strongly nonequilibrium conditions;[39] however, the overall trend can be well captured. In this sense, using the geometric average of T_{tr} and T_{v} with the power of 0.5 as the controlling temperature is relevant and thus adopted here to account for the effect of vibrational nonequilibrium on a single-step reaction.

For the modeling of the energy transfer rate r_ε between the translational–rotational mode and the vibrational mode, the Landau–Teller model is utilized in this paper as

$$\frac{D\varepsilon}{Dt} = r_\varepsilon = \frac{\varepsilon^{eq} - \varepsilon}{\tau_{\mathrm{v}}}, \tag{6}$$

where τ_{v} is the vibrational relaxation time scale. ε^{eq} is the equilibrium vibrational energy, which is associated with the local translational–rotational energy [thus, the corresponding value can be obtained by replacing T_{v} with T_{tr} in Eq. (3)]. Note that the total vibrational energy equation for both the reactant and product is considered such that there is no vibrational–vibrational energy exchange in the source term. Furthermore, the addition or removal of the vibrational energy due to chemical reactions is also eliminated by using a single η (or $\bar{\phi}$) and the nonpreferential model,[40] which assumes

Published under license by AIP Publishing

that molecules are created or destroyed at the average vibrational energy. Within the reaction zone, the corresponding T_v in each time step can be iterated through Newton's method with the known ε and T_{tr}.

Notably, following the stability analysis by Short and Stewart,[15] the density, pressure, temperature, and velocity in the above equations are normalized with respect to the corresponding dimensional thermodynamic properties and sound speed ($\overline{c_s}$) at the post-shock state (subscript as s) in an appropriately defined steady detonation wave. For the length scale, the steady half-reaction length $\mathcal{L}_{1/2}$ is chosen for normalization, which is defined as the distance from the shock to the point where half of the reactant is consumed under the equilibrium condition, and for time, $\mathcal{L}_{1/2}/\overline{c_s}$. Note that the frozen vibrational energy state is introduced right behind the shock, and the vibrational–chemical coupling is activated as the flow moves inward [the same state assumption is presented in Eq. (11) later]. The scaled activation energy ϑ, heat release β, and characteristic vibrational temperature η are defined as

$$\vartheta = \frac{\gamma \bar{E}_a}{\overline{c_s}^2}, \beta = \frac{\gamma \bar{Q}}{\overline{c_s}^2}, \eta = \frac{\bar{\phi}}{\overline{T_s}} \tag{7}$$

for dimensional activation energy $\bar{E}_a$, heat release $\bar{Q}$, and characteristic vibrational temperature $\bar{\phi}$.

Meanwhile, in this study, a time ratio $\tau^{c/v}$ discussed in the work of Uy *et al.*[34,35] is adopted again to demonstrate different degrees of vibrational nonequilibrium and is defined as follows:

$$\tau^{c/v} \equiv \frac{\tau_c}{\tau_v}, \tag{8}$$

where τ_c denotes the time needed for one-half of the reactant to be consumed and is a fixed chemical reaction time scale depending on the parameters in the chemical model. Accordingly, τ_v can be determined by varying $\tau^{c/v}$ during the analysis.

Although using the post-shock state parameters for scaling can provide a better description of the detonation structure and the stability behavior than using the pre-shock state, which has been illustrated in the work of Short and Stewart,[15] the scaled activation energy, heat release, and characteristic vibrational temperature by the pre-shock state quantities, E_a, Q, and ϕ, introduced by Erpenbeck,[12] will be adopted for a clear demonstration of the results in Secs. III and IV because E_a, Q, and ϕ will be independent of the detonation speed. E_a, Q, and ϕ are defined as

$$E_a = \frac{\gamma \bar{E}_a}{\overline{c_0}^2}, Q = \frac{\gamma \bar{Q}}{\overline{c_0}^2}, \phi = \frac{\bar{\phi}}{\overline{T_0}}, \tag{9}$$

where $\overline{c_0}$ and $\overline{T_0}$ are the dimensional pre-shock sound speed and pre-shock temperature, respectively. Notably, the same practice of using the definitions of Erpenbeck[12] for detonation stability presentation has also been implemented in their work.[15]

B. The steady one-dimensional solution

A steady one-dimensional solution can be obtained through the Rankine–Hugoniot analysis of the reactive flow model presented in Subsection II A. For convenience, a superscript * is added to specify the steady variables. Following the analysis by Erpenbeck[12] and He *et al.*,[41] the Rayleigh line and the Hugoniot curve can be derived by integrating Eq. (1) at the steady state. Assuming that the steady detonation propagates to the left at a speed of D_s^* (normalized by the dimensional post-shock sound speed $\overline{c_s}$), the corresponding flow path at the shock-attached coordinate system can be described as $X = x^l + D_s^* t^l$. The flow Mach number M_s^* right behind the shock can then be formulated as

$$M_s^{*2} = \frac{(\gamma-1)M^{*2}+2}{2\gamma M^{*2}-(\gamma-1)}, \tag{10}$$

where M^* is the detonation Mach number normalized by the dimensional pre-shock sound speed $\overline{c_0}$ of the initial reactants.

The corresponding steady variables immediately behind the shock are given as the shock boundary conditions as follows:

$$v^* = p^* = T^* = 1, \quad u^* = M_s^*, \quad \lambda^* = 0, \quad \varepsilon^* = 0. \tag{11}$$

Note that ε^* is assumed to be 0 such that the vibrational energy mode of reactants is activated immediately after the shock. By applying these dimensionless variables, the Rankine–Hugoniot relation is rewritten accordingly in terms of the specific volume v^* and pressure p^* across the shock profile and is presented in the following (nondimensionalized with respect to the post-shock state):

$$v^* = \frac{\gamma M_s^{*2}+1}{M_s^{*2}(\gamma+1)}\left[1 \mp w\xi\left(\lambda^*, \varepsilon^*\right)\right], \tag{12}$$

$$p^* = \frac{\gamma M_s^{*2}+1}{\gamma+1}\left[1 \pm \gamma w\xi\left(\lambda^*, \varepsilon^*\right)\right], \tag{13}$$

$$\xi\left(\lambda^*, \varepsilon^*\right) = \sqrt{1+\frac{\varepsilon^* - \lambda^*\beta}{\Omega}}, \Omega = \frac{\gamma\left(1-M_s^{*2}\right)^2}{2M_s^{*2}\left(\gamma^2-1\right)}, w = \frac{1-M_s^{*2}}{\gamma M_s^{*2}+1}. \tag{14}$$

The change in λ^* and ε^* across the profile can be evaluated by a single-step Arrhenius model with the two-temperature model and the Landau–Teller relaxation equation, i.e., Eqs. (4)–(6), respectively. The roots with $\mp$ signs in Eq. (12) [$\pm$ signs in Eq. (13), correspondingly] denote the strong and weak detonation solutions, respectively. In this study, strong detonation solution is adopted.

To specify a detonation with different degrees of overdrive, the detonation velocity D^* is determined as follows:

$$f = \left(\frac{D^*}{D_{CJ}^*}\right)^2, \tag{15}$$

where D_{CJ}^* is the Chapman–Jouguet (CJ) detonation velocity at the equilibrium state evaluated in terms of γ and Q. The newly established Zel'dovich–von Neumann–Döring (ZND) profile with vibrational energy included is then fully defined.

Figure 1 shows changes in variables across the steady CJ detonation wave with $Q = 50$ (or $\beta = 10.39$), $E_a = 50$ (or $\vartheta = 10.39$), $\gamma = 1.2$, $\phi = 20$ (or $\eta = 4.16$), and $f = 1$. The vibrational equilibrium case (eq) and nonequilibrium cases (Neq) at $\tau^{c/v} = 3$, 5, and 7 are selected for demonstration. The equilibrium case (eq) serves as a reference with an immediate establishment of vibrational equilibrium right after the shock, and therefore, the two temperatures T_{tr}^* and T_v^* are identical across the profile (equal to 1 at $X = 0$ as

Published under license by AIP Publishing

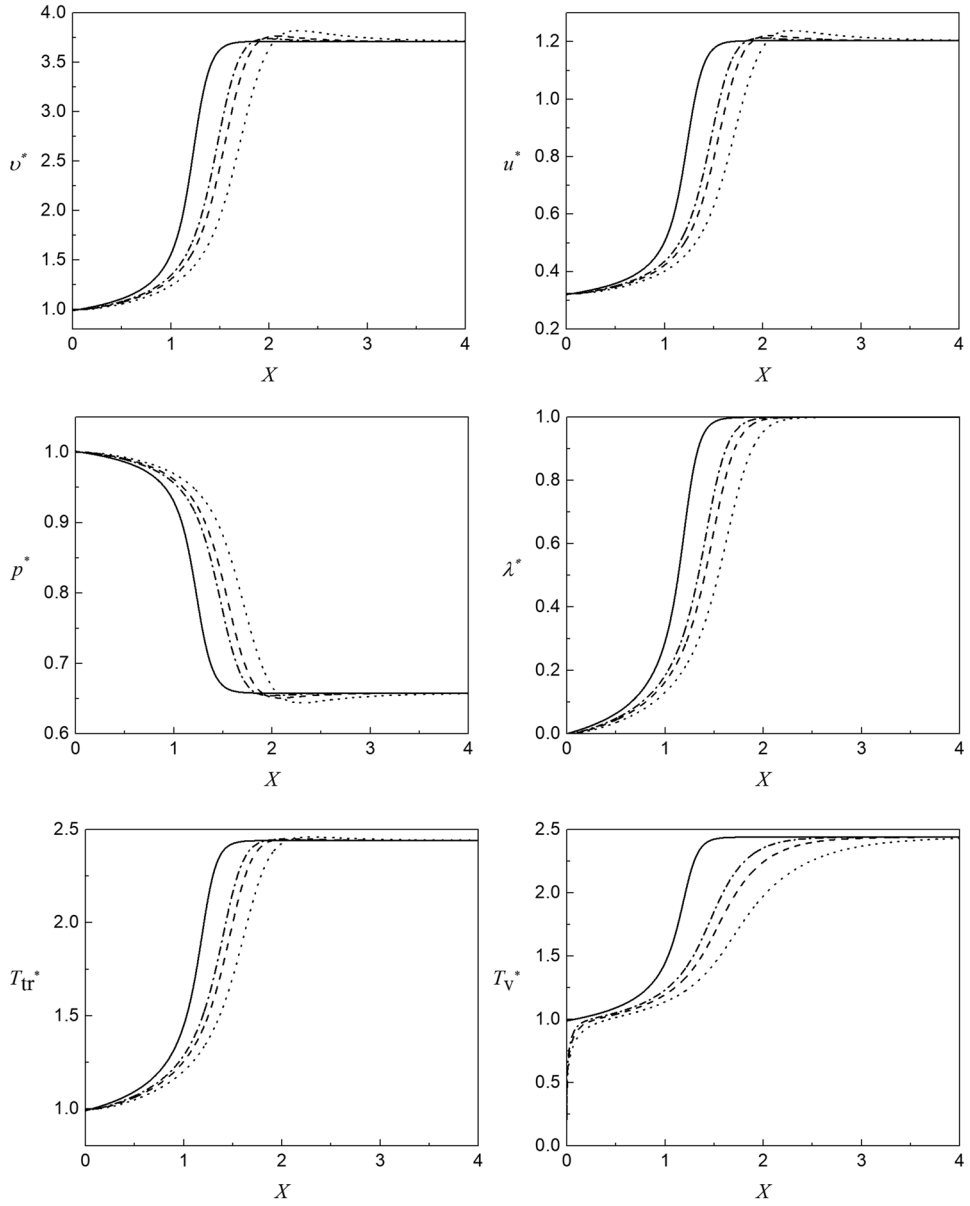

FIG. 1. Steady ZND profiles for $Q = 50$, $E_a = 50$, $\gamma = 1.2$, $\phi = 20$, and $f = 1$ for the vibrational equilibrium case (*eq*; solid curve) and nonequilibrium cases (*Neq*) with $\tau^{c/v} = 3$ (dotted curve), $\tau^{c/v} = 5$ (dashed curve), and $\tau^{c/v} = 7$ (dashed-dotted curve).

shown). However, the $T_v{}^*$ profile starts from 0 at $X = 0$ for other $\tau^{c/v}$ cases, as the vibrational mode is assumed to be excited only after the shock is encountered in these profiles. Recalling the definition of $\tau^{c/v} \equiv \tau_c/\tau_v$ in Eq. (8), a small $\tau^{c/v}$ implies that the detonation is under significant vibrational nonequilibrium and vice versa, which can be manifested in terms of the slowest chemical reaction rate by λ^* in the ZND profile at $\tau^{c/v} = 3$ compared with the other cases. Note that the asymptotic solutions at the downstream state and the initial upstream values remain the same for all cases because the change in $\tau^{c/v}$ will vary the steady detonation wave structure within the zone but not the end state or initial state properties.

C. One-dimensional linear stability analysis

A normal mode linear stability analysis for the steady detonation solution has been conducted by introducing one-dimensional perturbations. A shock-attached coordinated system is first defined as follows:

$$x = x^l + D_s^* t^l - \psi(t), \tag{16}$$

where $\psi(t)$ represents the perturbation to the shock location. Perturbations to the steady detonation structure are then sought in the following forms:

$$z = z^*(x) + z'(x)\exp(\alpha t), \quad \psi = \psi' \exp(\alpha t), \tag{17}$$

Published under license by AIP Publishing

where

$$z = [v, u, p, \lambda, \varepsilon]^{\mathrm{T}}. \tag{18}$$

Re(α) represents the growth rate of the disturbance, whereas Im(α) represents the frequency of the disturbance. The linearized perturbation equations for the complex perturbation eigenfunction $z'(x)$ are then constructed by substituting (16) and (17) into Eqs. (1)–(7) (normalized with the post-shock parameters) and are written in the following forms:

$$\boldsymbol{A}^* \zeta_x + \left(\alpha \cdot \boldsymbol{I} + \boldsymbol{C}^*\right)\zeta - \alpha z_x^* = 0, \tag{19}$$

$$\zeta = z'/\psi', \tag{20}$$

where $\boldsymbol{I}$ is the identity matrix and the matrices $\boldsymbol{A}^*$ and $\boldsymbol{C}^*$ are expressed as

$$\boldsymbol{A}^* = \begin{bmatrix} u & -v & 0 & 0 & 0 \\ 0 & u & v/\gamma & 0 & 0 \\ 0 & \gamma p & u & 0 & 0 \\ 0 & 0 & 0 & u & 0 \\ 0 & 0 & 0 & 0 & u \end{bmatrix}^*, \tag{21}$$

$$\boldsymbol{C}^* = \begin{bmatrix} -u_x & v_x & 0 & 0 & 0 \\ p_x/\gamma & u_x & 0 & 0 & 0 \\ C_{31} & p_x & C_{33} & C_{34} & C_{35} \\ -r_v & \lambda_x & -r_p & -r_\lambda & -r_\varepsilon \\ -r_{\varepsilon,v} & \varepsilon_x & -r_{\varepsilon,p} & 0 & -r_{\varepsilon,\varepsilon} \end{bmatrix}^*, \tag{22}$$

where

$$C_{31} = \frac{(\gamma-1)}{v}\left[\frac{\beta r - r_\varepsilon}{v} - (\beta r_v - r_{\varepsilon,v})\right], \tag{23}$$

$$C_{33} = \gamma u_x - \frac{(\gamma-1)}{v}(\beta r_p - r_{\varepsilon,p}),$$

$$C_{34} = -\frac{(\gamma-1)}{v}\beta r_\lambda,$$

$$C_{35} = \frac{(\gamma-1)}{v}(r_{\varepsilon,\varepsilon} - \beta r_\varepsilon).$$

The derivatives of $r(v, p, \lambda, \varepsilon)$ [i.e., Eq. (4)] in $\boldsymbol{C}^*$ are

$$r_v = \frac{r\vartheta}{2vT_{avg}}, \quad r_p = \frac{r\vartheta}{2pT_{avg}}, \tag{24}$$

$$r_\lambda = -K\exp\left(-\frac{\vartheta}{T_{avg}}\right), \quad r_\varepsilon = \frac{\partial r}{\partial T_{\mathrm{v}}} \cdot \frac{\partial T_{\mathrm{v}}}{\partial \varepsilon},$$

where

$$\frac{\partial r}{\partial T_{\mathrm{v}}} = \frac{r\vartheta}{2T_{\mathrm{v}}T_{avg}}, \quad \frac{\partial T_{\mathrm{v}}}{\partial \varepsilon} = \frac{T_{\mathrm{v}}^2[\exp(\phi/T_{\mathrm{v}}) - 1]^2}{\phi^2 \exp(\phi/T_{\mathrm{v}})}.$$

The derivatives of $r_\varepsilon(v, p, \varepsilon)$ [i.e., Eq. (6)] in $\boldsymbol{C}^*$ are

$$r_{\varepsilon,v} = \frac{\delta}{\tau_{\mathrm{v}} v}, \quad r_{\varepsilon,p} = \frac{\delta}{\tau_{\mathrm{v}} p}, \quad r_{\varepsilon,\varepsilon} = -\frac{1}{\tau_{\mathrm{v}}}, \tag{25}$$

$$\delta = \frac{\phi^2}{pv}\frac{\exp(\phi/pv)}{[\exp(\phi/pv) - 1]^2}.$$

From the linearization of the Rankine–Hugoniot shock relation, the perturbation shock condition is derived as follows:

$$v' = \frac{4\alpha}{(\gamma+1)M^{*2}M_s^*}\psi', \quad u' = \frac{2\left(1 + M^{*2}\right)\alpha}{(\gamma+1)M^{*2}}\psi', \tag{26}$$

$$p' = -\frac{4\gamma M_s^* \alpha}{\gamma+1}\psi', \quad \lambda' = 0, \varepsilon' = 0$$

which can be expressed in terms of ζ [Eq. (20)],

$$\zeta(0) = \left[\frac{4\alpha}{(\gamma+1)M^{*2}M_s^*}, \frac{2\left(1 + M^{*2}\right)\alpha}{(\gamma+1)M^{*2}}, -\frac{4\gamma M_s^* \alpha}{\gamma+1}, 0, 0\right]^{\mathrm{T}}. \tag{27}$$

Finally, a boundary condition is applied at the end of the reaction zone such that no acoustic wave propagates upstream from infinity.[9,15] This acoustic radiation condition[42] is illustrated in the form of

$$u' - \frac{v_b^*}{\gamma c_b^*}p' = 0, \tag{28}$$

which again can be expressed by the second and third terms of ζ,

$$\zeta_2(\infty) - \frac{v_b^*}{\gamma c_b^*}\zeta_3(\infty) = 0, \tag{29}$$

where v_b^* and c_b^* are the unperturbed specific volume and isentropic sound speed in the burned reactant. This condition is implemented when λ^* approaches 1 at $x = \infty$, where the detonation with the present vibrational–chemical coupling model should reach the equilibrium state.

To solve the linearized perturbation equations in Eq. (19) and determine the complex eigenvalues α and eigenfunction $z'(x)$, a two-point boundary value solution technique is adopted based on the numerical shooting method described in Lee and Stewart.[13] The shooting begins from an initial guess of α and then, with the given initial condition in Eqs. (27) and (19), is integrated from the shock position toward the end state denoting the equilibrium point in the reaction zone. A two-variable Newton–Raphson iteration is applied such that α is iterated until the acoustic radiation condition in Eq. (28) is satisfied. A tolerance of 10^{-7} in real eigenfunctions at the boundary is allowed in this study.

III. NUMERICAL METHOD

One of the important results obtained from LSA is the neutral stability limit. To verify the results near the stability boundary based on this analytical approach, the numerical simulation is utilized in this study such that the results from the two approaches can be compared. With the steady ZND solution discussed in Subsection II B as the given initial condition, the reactive Euler equation, i.e., Eq. (1), is integrated numerically by the conservation element and solution element (CE/SE) scheme with second-order accuracy.[43] This numerical scheme has a characteristic of unifying the treatment of both

Published under license by AIP Publishing

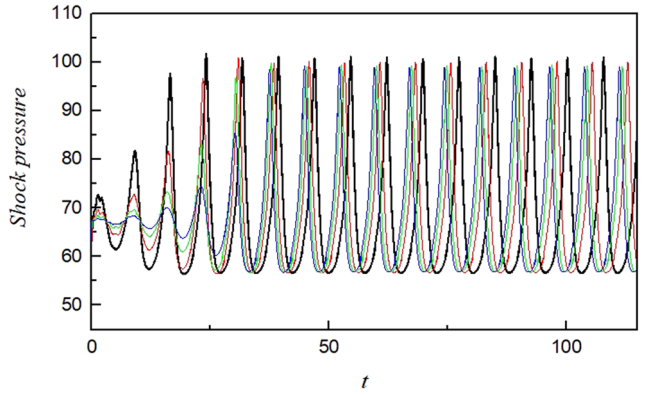

FIG. 2. Shock pressure history of one-dimensional piston-supported detonation with $Q = 50$, $E_a = 50$, $\gamma = 1.2$, and $f = 1.6$ for grid resolutions of $10/\mathcal{L}_{1/2}$ (black solid curve), $20/\mathcal{L}_{1/2}$ (red dotted curve), $40/\mathcal{L}_{1/2}$ (green dashed curve), and $80/\mathcal{L}_{1/2}$ (blue dashed-dotted curve), respectively.

space and time and thus has been applied extensively in the fields of gaseous detonation,[30,44] hypersonic flows,[45–48] and shock/droplet (bubble) interactions.[49–54]

Based on the study by Sharpe and Falle[19] on the convergence of the stability boundary, an effective numerical grid resolution of 128 points per half-reaction zone length ($128/\mathcal{L}_{1/2}$) was implemented to resolve the detonation wave structure. Similar to their work, a zero gradient condition was applied at the boundary with at least 1000 $\mathcal{L}_{1/2}$ behind the initial shock position so that the boundary effect was eliminated.

For validation of the code, a case of piston-supported detonation in one dimension reported by Shen and Parsani[55] was simulated, with $Q = 50$, $E_a = 50$, $\gamma = 1.2$, and $f = 1.6$, as shown in Fig. 2. The percentage errors of the periods of oscillation computed in our code compared with those from tje study of Shen and Parsani[55] for grid resolutions of $10/\mathcal{L}_{1/2}$, $20/\mathcal{L}_{1/2}$, $40/\mathcal{L}_{1/2}$, and $80/\mathcal{L}_{1/2}$ do not exceed 0.01%. Good validation is demonstrated.

IV. STABILITY ANALYSIS RESULTS

Based on the algorithm developed in Sec. II, a comparison of the normal mode result with that in the literature is presented in Subsection IV A first. Then, parametric studies on the change in the activation energy E_a, the degree of overdrive f, the characteristic vibrational temperature ϕ, and the heat release Q are presented in Subsections IV B–IV E, respectively. Fianlly, the result from LSA is compared with that computed by numerical simulation in Subsection IV F for validation.

A. Comparison of normal mode result with literature

As discussed in the work of Kabanov and Kasimov,[56] the results obtained from the LSA in terms of complex eigenvalues vary with different scales in works of other researchers, although they share the same physical interpretation. In this section, a comparison of the unstable spectra for fundamental modes between the present work (following the scales by Short and Stewart[15]) and the normal-mode results from the literature is presented for parameters $\gamma = 1.2$, $Q = 50$, and $f = 1$ under the thermal equilibrium state [without considering the existence of vibrational energy ε in Eq. (2)].

TABLE I. Comparison of the unstable spectra for the fundamental modes between the present work and the normal mode results summarized in Erpenbeck scales at $\gamma = 1.2$, $Q = 50$, and $f = 1$. The corresponding eigenvalues α consist of the real part [i.e., Re(α)] and the imaginary part [i.e., Im(α)].

	Present work based on Short and Stewart scales[15]		Results of Kabanov and Kasimov[56] in Erpenbeck scales	
E_a	Re(α)	Im(α)	Re(α)	Im(α)
50	0.726	0.000	1.743	0.000
	0.039	0.000	0.084	0.000
26	0.016	0.218	0.037	0.522
25.26	0.000	0.220	0.000	0.530

Table I shows the comparison of the results at the selected E_a range. Referring to the study by Sharpe,[14] the eigenvalues of this particular parameter setting would split into two purely real eigenvalues at $E_a > 35$ in which one would go to zero asymptotically and the other one would increase as E_a increases. Therefore, the fundamental mode consists of two sets of eigenvalues at $E_a = 50$. By comparing the eigenvalues obtained in the two scales, the conversion factor from the present work to the factor summarized by Kabanov and Kasimov in the Erpenbeck scale is ~2.4. Based on the analysis by Kabanov and Kasimov,[56] the conversion factor can be deduced from the ratio of the nondimensional pre-exponential factor K in both scales. Following their approaches, the numerical value of this factor is evaluated to be 2.403, which fits with the estimation from the corresponding eigenvalues obtained with the two scales here. Note that part of the data [i.e., values of Re(α) and Im(α)] obtained in the present work has been compared with that in the work of Short and Stewart[15] on the two-dimensional linear stability analysis to ensure that the results are validated.

As mentioned in Subsection II A above, the difference of the scale in the present work from the Erpenbeck scale is that the latter scale is nondimensionalized with the pre-shock state parameters. Although the use of the post-shock state for normalization is better in describing the detonation structure, the eigenvalues obtained in the Erpenbeck scales near the stability boundary can closely predict the disturbance frequency. For instance, based on the Im(α) obtained at the neutral stability limit $E_a = 25.26$ in LSA, the period of oscillation in this case is expected to be $2\pi/0.53 = 11.855$, which is fairly close to the averaged period of oscillation determined from the same case using the numerical simulation, i.e., 11.860. In this context, the interpretation of the results in Erpenbeck scales is also included in the following discussion as necessary.

B. Linear spectrum migration by varying activation energy at different $\tau^{c/v}$

Figure 3 shows the relationship of the frequency and the growth rate of the fundamental mode and first overtone in terms of the imaginary part and the real part of the eigenvalue, respectively. Additionally shown is the dependence of the growth rate on E_a at $\tau^{c/v} = 3$ and $\tau^{c/v} = 5$ with $\gamma = 1.2$, $Q = 50$, $\phi = 20$, and $f = 1$. For the

Published under license by AIP Publishing

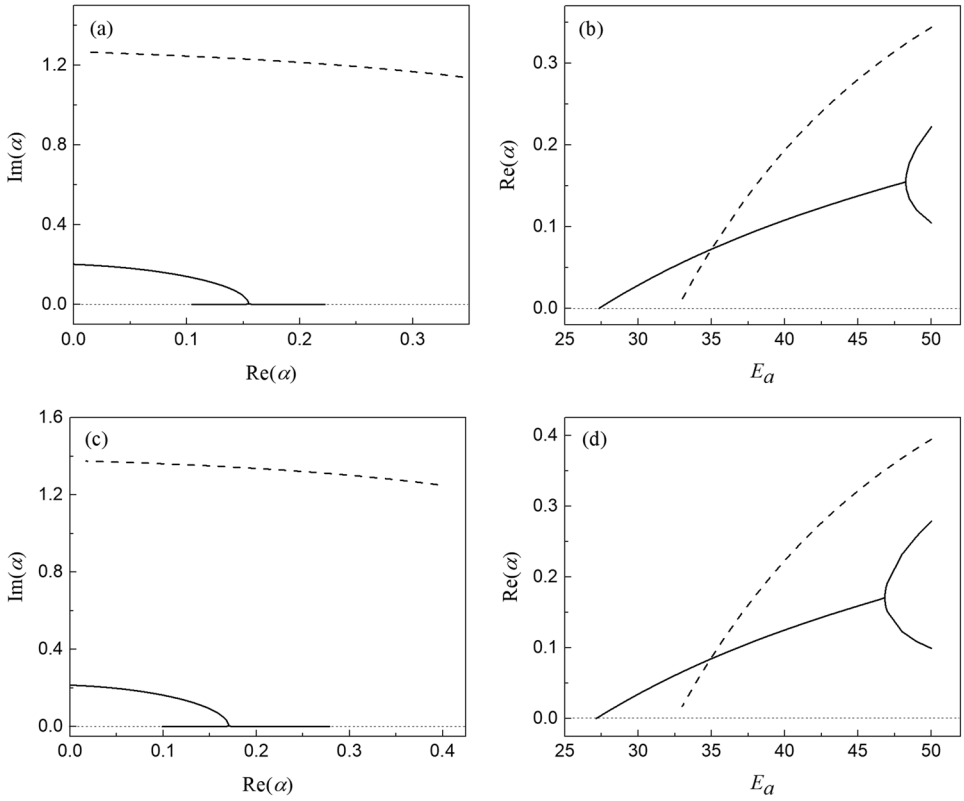

FIG. 3. Stability spectrum showing (a) Im(α) vs Re(α) and (b) Re(α) vs E_a for $\tau^{c/v}$ = 3 and (c) Im(α) vs Re(α) and (d) Re(α) vs E_a for $\tau^{c/v}$ = 5. The solid curve represents the fundamental mode, and the dashed curve represents the first overtone. γ = 1.2, Q = 50, ϕ = 20, and f = 1.

fundamental mode, the neutral stability limit (denoted as the zero growth rate) is at E_a = 27.32 for the case of $\tau^{c/v}$ = 3, whereas the corresponding limit is at E_a = 27.12 for the case of $\tau^{c/v}$ = 5, below which the detonation is stable under the one-dimensional perturbation. As E_a increases, the growth rate increases accordingly, while the corresponding frequency approaches zero at E_a = 48.25 and E_a = 46.82 for $\tau^{c/v}$ = 3 and $\tau^{c/v}$ = 5, respectively. A further increase in E_a from these points would lead to the bifurcation of the fundamental eigenmode into two real nonoscillatory eigenvalues—one that decreases asymptotically to zero and the other that increases with E_a. The overall features in these stability spectra are qualitatively the same with the linear stability analysis of idealized detonation.[14] However, both the neutral stability limit and the bifurcation point are shifted. The change in the limit can be attributed to the additional energy exchange mechanism for vibrational relaxation in Eq. (6) and thus leads to the change in the reaction rate along the profile overall. Nevertheless, the change from one oscillatory mode to two nonoscillatory modes or vice versa along the spectra is always captured, and the reason is that we are using the same Arrhenius reaction model to describe the product and heat formation in the linear stability analysis. The similarity in stability behavior could also be found in the LSA related to pathological detonation, where an endothermic reaction in Arrhenius form is added in the system instead.[16]

The behavior of the first overtone is relatively different from that of the fundamental mode. As presented by the dashed lines in Fig. 3, the growth rate of the first overtone increases with reducing frequency when E_a is beyond its neutral stability limit. No bifurcation of eigenvalues is shown in this mode throughout the selected E_a range. By comparing the stability spectra between the fundamental mode and the first overtone, the growth rate of the first overtone always has a steeper slope as E_a increases. In addition, migrations of the curves are observed at different $\tau^{c/v}$ cases. For instance, the frequency is 1.27 for $\tau^{c/v}$ = 3 at E_a = 33, whereas it is 1.37 for $\tau^{c/v}$ = 5 at the same E_a. Nevertheless, the overall trends are similar as $\tau^{c/v}$ varies. From the previous finding by Sharpe (1999), the presence of the first overtone is also observed in the linear stability analysis of pathological detonation considering one-dimensional perturbation. It is expected that more high frequency modes are observed in the case with two-dimensional perturbations. Nevertheless, the main focus in this work is on the longitudinal instability only, and thus, further high frequency modes would not be discussed here.

Regarding the neutral stability limit captured in the fundamental mode, Fig. 4 shows the relationship of the imaginary part and the real part of eigenvalues and the dependence of the growth rate on E_a in the range of $25 < E_a \leq 50$ at $\tau^{c/v}$ = 3, 5, 7, 9, 275, and 700. As seen, the neutral stability limit [i.e., Re(α) = 0] shifts to a higher E_a value as $\tau^{c/v}$ decreases. Recalling the definition of $\tau^{c/v} \equiv \tau_c/\tau_v$ in Eq. (7), this implies that under the same activation energy E_a, the growth rate of the fundamental mode decreases when vibrational relaxation is significant. In other words, the detonation is stabilized at lower $\tau^{c/v}$. On the other hand, the bifurcation point at which the unstable mode splits into two [i.e., Im(α) = 0] moves to a smaller Re(α) as

Published under license by AIP Publishing

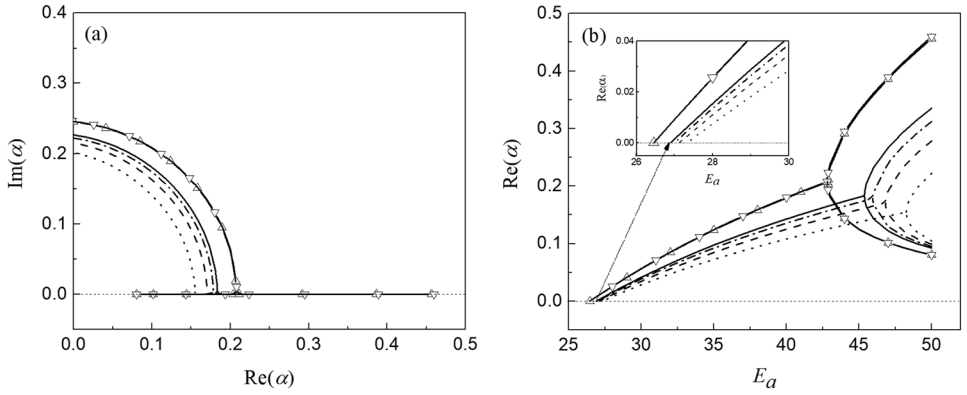

FIG. 4. Stability spectrum showing (a) Im(α) vs Re(α) and (b) Re(α) vs E_a with the fundamental mode only at $\tau^{c/v}$ = 3 (dotted curve), $\tau^{c/v}$ = 5 (dashed curve), $\tau^{c/v}$ = 7 (dashed-dotted curve), $\tau^{c/v}$ = 9 (solid curve), $\tau^{c/v}$ = 275 (solid-Δ curve), and $\tau^{c/v}$ = 700 (solid-∇ curve). γ = 1.2, Q = 50, ϕ = 20, and f = 1.

$\tau^{c/v}$ decreases. This indicates that splitting occurs at a lower growth rate, also implying that detonation is stabilized under significant vibrational nonequilibrium.

From the stability analysis in the previous literature,[13,14] it is found that the mechanism of detonation instability is related to the induction time scale and a longer induction time tends to bring about the detonation instability. More recent work by Ng *et al.*[57] revealed that the detonation stability is sensitive not only to the induction process but also to the reaction process involving energy deposition. A stability parameter χ was introduced in their work, which is proportional to the ratio of induction length Δ_I to the exothermic reaction length Δ_R. If the ratio χ is small, a stable system is presented and vice versa. In the meanwhile, from the analysis by Uy *et al.*[34] based on the same chemical–vibrational coupling mechanism used in this paper, an increase in the half-reaction length (thus Δ_R) is always observed when $\tau^{c/v}$ decreases, and the induction time length shows little change with $\tau^{c/v}$. Therefore, the computed $\chi \propto \Delta_I/\Delta_R$ should be smaller compared to the case of vibrational equilibrium. The increase in the half-reaction length with decreasing $\tau^{c/v}$ can be also seen in the λ^* profile of Fig. 1 above. Apparently, the half-reaction length is elongated and the chemical reaction is in a much gradual manner under vibrational nonequilibrium. By using the concept of stability parameter χ in the analysis, the stabilization effect of vibrational relaxation on detonation is explained. The sensitivity of detonation instability to temperature fluctuations also become smaller under the state of vibrational nonequilibrium due to the presence of energy mode exchange between the translational–rotational mode and vibrational mode. Consequently, the flow instability is more resistant to the disturbance.

For the case of $\tau^{c/v}$ = 275 and $\tau^{c/v}$ = 700, the two stability spectra overlapped with each other in Fig. 4. Indeed, both the stability limit and the bifurcation point in the spectrum remain unchanged when $\tau^{c/v} > 275$. The assumption of the thermal equilibrium state should then be valid beyond this critical time ratio, and the corresponding neutral stability limit is found at E_a = 26.45.

C. Linear spectrum migration by varying the overdriven factor at different $\tau^{c/v}$

An increase in the degree of overdrive f in both numerical simulation and LSA is known to be crucial in stabilizing detonation propagation and has been reported in the literature.[13,25] Therefore, a variation in the stability spectrum with f for the selected $\tau^{c/v}$ is examined in this section and is presented in Fig. 5 with γ = 1.2, Q = 50, ϕ = 20, and E_a = 50. As expected, the detonation becomes stable at large f, and the corresponding neutral stability limit for the fundamental mode is at f = 1.555 for $\tau^{c/v}$ = 5 and at f = 1.582 for $\tau^{c/v}$ = 10. Initially, two unstable nonoscillatory modes are observed at f = 1. As f increases, the two unstable modes converge to a single unstable eigenmode, which becomes oscillatory [i.e., with Im(α) > 0]. The convergence points for $\tau^{c/v}$ = 5 and $\tau^{c/v}$ = 10 are at f = 1.0292 and f = 1.0488, respectively. With further increases in f, the growth rate of the unstable mode decreases asymptotically to zero, whereas the frequency increases until the neutral stability limit is reached. The overall stability behavior is similar to that displayed in Subsection IV B, but the trend is developed in the opposite way.

Considering the stability spectrum for the first overtone, the corresponding growth rate decreases almost linearly to zero as f increases, with a decay rate much faster than that of the fundamental mode. In contrast to the tendency with varying E_a (Subsection IV B), the frequency increases slightly with decreasing growth rate.

To closely examine the migration of the stability spectra for the fundamental mode under different $\tau^{c/v}$, the studied cases (i.e., $\tau^{c/v}$ = 5, 10, 20, 252 and 700) are grouped and presented in Fig. 6, under a range of $1 \le f \le 1.7$. Generally, the decrease in $\tau^{c/v}$ shifts the neutral stability limit to lower f. In other words, the detonation is stabilized due to the vibrational nonequilibrium effect under the same f. Moreover, a shift of the convergence point to smaller Re(α) at lower $\tau^{c/v}$ is observed in the dependence of the growth rate and the frequency of the fundamental mode in Fig. 6(a), and thus, the stabilization under the vibrational nonequilibrium effect is further revealed. In summary, it is shown again that the decrease in $\tau^{c/v}$ can stabilize the detonation propagation, and the presence of vibrational nonequilibrium would lead to the decrease in the stability limit in f.

Finally, two cases of very large $\tau^{c/v}$ (i.e., $\tau^{c/v}$ = 252 and 700) are presented in the same figure, and the overlapping of these two spectra indicates that no further shift of the limit is identified if τ_c is much larger than τ_v. Above $\tau^{c/v}$ = 252 for these particular parameter sets, the detonation can be treated as in the thermal equilibrium state

Published under license by AIP Publishing

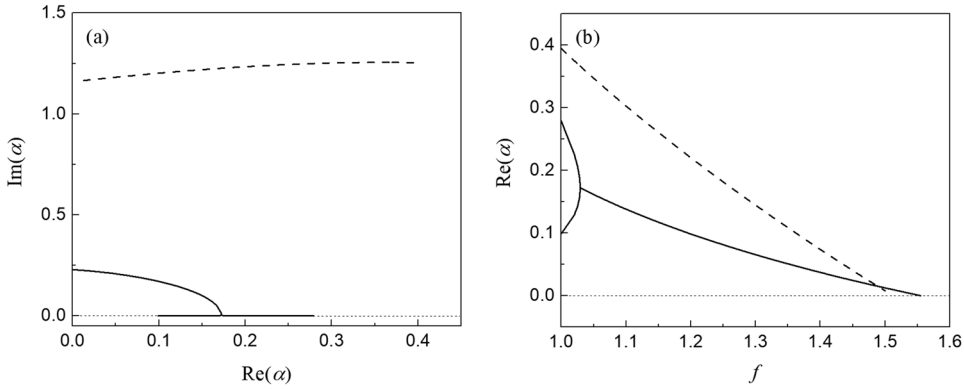

FIG. 5. Stability spectrum showing (a) Im(α) vs Re(α) and (b) Re(α) vs f for $\tau^{c/v}$ = 5 and (c) Im(α) vs Re(α) and (d) Re(α) vs f for $\tau^{c/v}$ = 10. The solid curve represents the fundamental mode, and the dashed curve represents the first overtone. γ = 1.2, Q = 50, ϕ = 20, and E_a = 50.

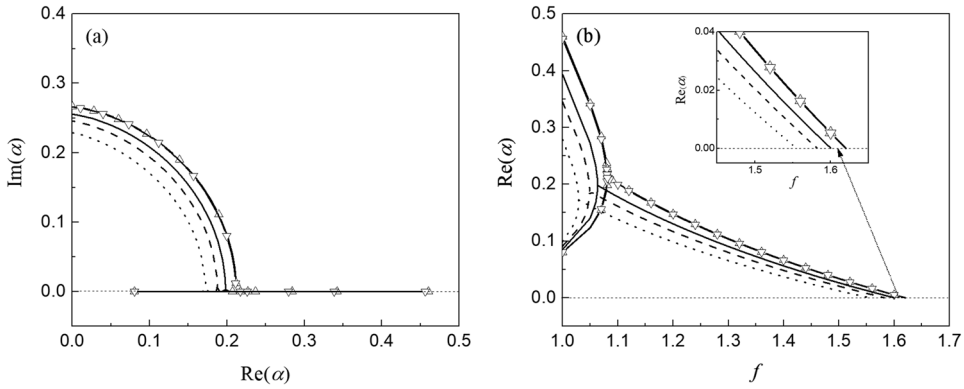

FIG. 6. Stability spectrum showing (a) Im(α) vs Re(α) and (b) Re(α) vs f with the fundamental mode only at $\tau^{c/v}$ = 5 (dotted curve), $\tau^{c/v}$ = 10 (dashed curve), $\tau^{c/v}$ = 20 (solid curve), $\tau^{c/v}$ = 252 (solid-Δ curve), and $\tau^{c/v}$ = 700 (solid-∇ curve). γ = 1.2, Q = 50, ϕ = 20, and E_a = 50.

throughout the reaction profile. The corresponding neutral stability limit is f = 1.62.

D. Linear spectrum migration by varying the characteristic vibrational temperature at different $\tau^{c/v}$

When the detonation is under vibrational nonequilibrium, vibrational temperature ϕ is used to characterize the vibrational energy content inside the system. The change in ϕ under different $\tau^{c/v}$ for the fundamental mode is therefore worth investigating in this study, and two unstable conditions are considered in the analysis with γ = 1.2, Q = 50, and f = 1: the case at E_a = 30, where only one unstable oscillatory mode exists, and the case at E_a = 50, where two nonoscillatory unstable modes are observed [see Fig. 4(b)].

Figure 7 shows the dependence of the growth rate on ϕ at E_a = 50 for $\tau^{c/v}$ = 5, 10, and 20. Since the unstable mode here is nonoscillatory, Im(α) is always zero under this condition. The difference in the growth rate between the two unstable modes is narrowed when ϕ decreases. The increase in $\tau^{c/v}$ generally moves the upper unstable mode to a higher level [for example, Re(α) = 0.45 for ϕ = 50 at $\tau^{c/v}$ = 5 and Re(α) = 0.58 for ϕ = 50 at $\tau^{c/v}$ = 20], while the influence on

Published under license by AIP Publishing

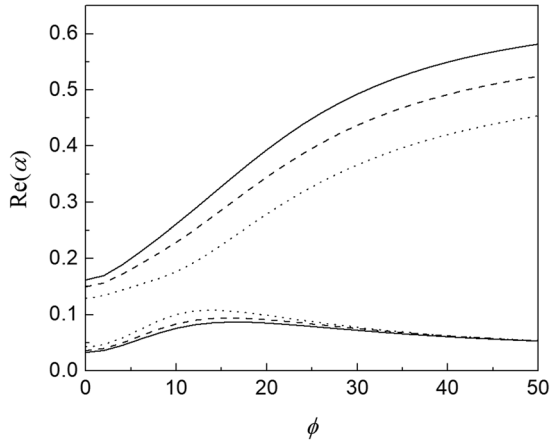

FIG. 7. Stability spectrum showing Re(α) vs ϕ with the fundamental mode only for $\tau^{c/v}$ = 5 (dotted curve), $\tau^{c/v}$ = 10 (dashed curve), and $\tau^{c/v}$ = 20 (solid curve). γ = 1.2, Q = 50, E_a = 50, and f = 1.

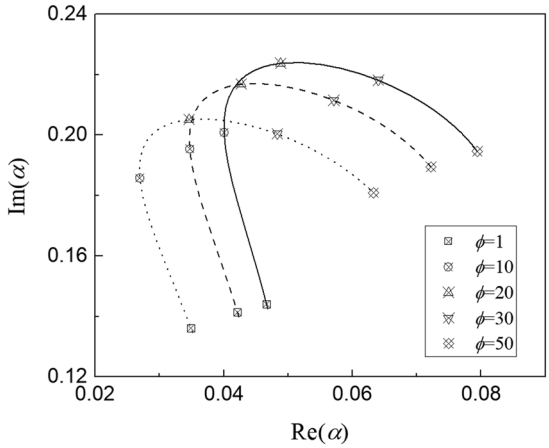

FIG. 8. Stability spectrum showing Im(α) vs Re(α) of the fundamental mode only for $\tau^{c/v}$ = 5 (dotted curve), $\tau^{c/v}$ = 10 (dashed curve), and $\tau^{c/v}$ = 20 (solid curve) in the range of ϕ from 1 to 50. γ = 1.2, Q = 50, E_a = 30, and f = 1.

the lower unstable mode is relatively weak. In particular, the change in the lower unstable mode is within 0.05 in the selected ϕ range for all three cases of $\tau^{c/v}$, but the change in the upper unstable mode can be over 0.5. In other words, the upper unstable mode is sensitive to the change in vibrational nonequilibrium, while the lower unstable mode is not. Referring to Sharpe's work on LSA in idealized detonation,[14] the larger value of Re(α) computed in the fundamental mode would always represent the maximum growth rate and become the most unstable mode. Therefore, the upper unstable mode dominates the denotation instability. The high sensitivity of the upper unstable mode to vibrational relaxation prevails. Additionally, the growth rate of the upper unstable mode is suppressed at low $\tau^{c/v}$, denoting that the detonation is again stabilized at the vibrational nonequilibrium state. Notably, although the convergence tendency of the growth rates for these two unstable eigenmodes along with the decrease in ϕ is similar to that in Fig. 4(b) (with E_a), they do not converge to a single one, even at ϕ = 1, which is very small.

For the case of a single oscillatory unstable mode near the stability limit, Fig. 8 shows the relationship between the frequency and growth rate at E_a = 30 for $\tau^{c/v}$ = 5, 10, and 20 with ϕ ranging from 1 to 50. Similar to the case at E_a = 50, no neutral stability limit is found under the selected ϕ range, but a minimum growth rate [or minimum Re(α)] of the fundamental mode is determined around ϕ = 10 for all three $\tau^{c/v}$ cases. Below this minimum growth rate, a further decrease in ϕ would lead to an increase in the growth rate again as the frequency [or Im(α)] decreases. Comparatively, the growth rate increases comparably faster if ϕ increases beyond the minimum growth rate point, with the frequency increases first and then decreases accordingly. In general, the stability spectrum shifts to higher Re(α) as $\tau^{c/v}$ increases, which again agrees with the observations in Fig. 4(b).

Recalling the definition of the vibrational relaxation mechanism in Eq. (6), the relaxation rate depends heavily on the vibrational time scale τ_v or the time ratio $\tau^{c/v}$ instead of ϕ in the analysis. The low sensitivity of the change in the half-reaction length to ϕ under the vibrational nonequilibrium state has been previously reported in the work of Uy *et al.*[34] Together with the findings in the two tested conditions, it is suggested that ϕ plays only a slight role in stabilizing the detonation whenever the state is under thermal nonequilibrium. Accordingly, no critical time ratio $\tau^{c/v}$ and no change in the number of unstable modes are determined in this part.

E. Neutral stability curve by varying the heat release at different $\tau^{c/v}$

The instability regime is always shown varying with the heat release Q in different literature studies,[13,15,56] and thus, the neutral stability curves relating Q with E_a and that of Q with f are presented in Figs. 9 and 10, respectively, with different $\tau^{c/v}$ cases ($\tau^{c/v}$ = 3, 7, and 700 for illustration), while γ = 1.2 and ϕ = 20 are fixed. In a typical Q–E_a neutral stability curve, the region outside the envelope of the curve is determined to be stable, whereas the region enclosed by the curve represents is unstable. It is similar for the case of a typical Q–f

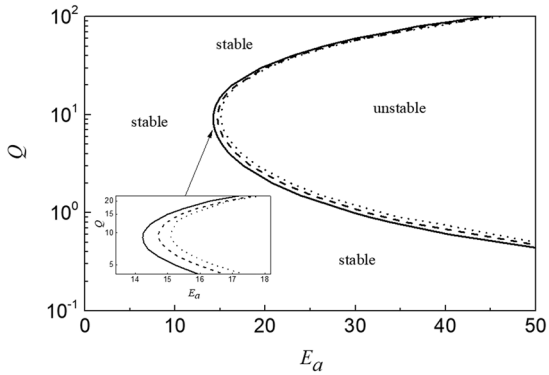

FIG. 9. The neutral stability curve with Q vs E_a at $\tau^{c/v}$ = 3 (dotted curve), $\tau^{c/v}$ = 7 (dashed curve), and $\tau^{c/v}$ = 700 (solid curve). γ = 1.2, ϕ = 20, and f = 1.

Published under license by AIP Publishing

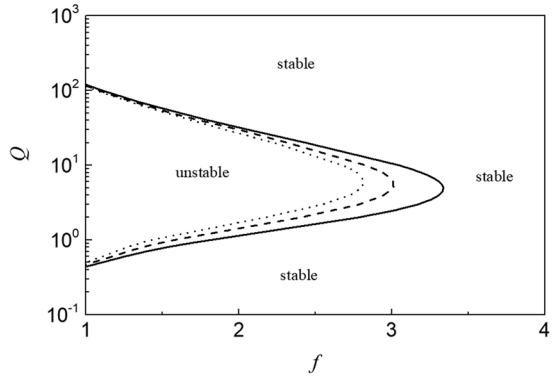

FIG. 10. The neutral stability curve with Q vs f at $\tau^{c/v}$ = 3 (dotted curve), $\tau^{c/v}$ = 7 (dashed curve), and $\tau^{c/v}$ = 700 (solid curve). γ = 1.2, ϕ = 20, and E_a = 50.

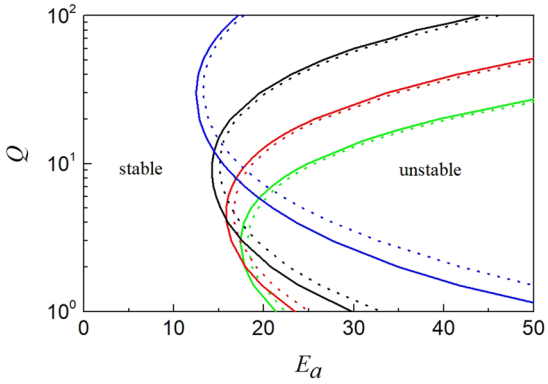

FIG. 11. The neutral stability curve with Q versus E_a at $\tau^{c/v}$ = 3 (dotted curve) and $\tau^{c/v}$ = 600 (solid curve) for γ = 1.1 (blue), γ = 1.2 (black), γ = 1.3 (red), and γ = 1.4 (green) respectively. ϕ = 20 and f = 1.

neutral stability curve. As discussed before, $\tau^{c/v} > 300$ (in this case would be $\tau^{c/v}$ = 600 or 700) is served as a reference to demonstrate the vibrational equilibrium case.

Referring to the inset of Fig. 9, the detonation is always stable below E_a = 14, which has also been determined in the previous literature.[13] On the other hand, for the Q–f neutral stability curves presented in Fig. 10, a stable condition is always found at above f = 3.5. Furthermore, it is illustrated that the unstable region becomes smaller across the selected Q range with decreasing $\tau^{c/v}$ in both Figs. 9 and 10. Also, the increase in critical E_a and the decrease in critical f as $\tau^{c/v}$ decreases are clearly seen. The critical points on the neutral stability curves in Fig. 9 for $\tau^{c/v}$ = 700, 7, and 3 are at Q = 10 and E_a = 14.25, 14.72, and 15.10, respectively, while those in Fig. 10 are at Q = 10 and f = 3.05, 2.83, and 2.68, respectively. In other words, in the low Q range (below 10) under vibrational nonequilibrium, larger amounts of exothermicity are required to generate instability by increasing the activation energy or decreasing degree of overdrive, while it is vice versa for the case in the high Q range.

It is known that the specific ratio γ is closely related to the types of molecules and the microscopic states of the molecules[37] (including the translational, rotational, and vibrational energy modes), and the effect of γ on the detonation stability under molecular vibrational equilibrium/nonequilibrium conditions is also examined here by comparing the corresponding neutral stability curves. Figure 11 shows the Q–E_a curves with different γ, i.e., γ = 1.1, 1.2, 1.3, and 1.4 under vibrational equilibrium ($\tau^{c/v}$ = 600) and vibrational nonequilibrium ($\tau^{c/v}$ = 3). As seen, for different γ, instability regions reduce when vibrational relaxation is considered (i.e., $\tau^{c/v}$ = 3). This implies that the vibrational nonequilibrium effect can always play a role in stabilizing the detonation, regardless of the types of molecules considered in the system. Further clarification on the detonation stability in different types of reactive flow systems will be provided with numerical simulations in the future.

Figure 12 shows the neutral curves relating Q with ϕ at different $\tau^{c/v}$, while γ = 1.2, f = 1, and E_a = 26. The stability behavior is quite different from that discussed in Figs. 9–11. The unstable region in Fig. 12 is bounded by the two neutral stability curves, while other regions are stable. As seen, the unstable region again becomes smaller when $\tau^{c/v}$ decreases, and the stabilization effect with the consideration of vibrational relaxation is identified. Moreover, the two neutral curves of $\tau^{c/v}$ = 3 and 7 almost lie horizontally throughout the selected ϕ range, indicating that the variation in ϕ would not bring a large change in the stability behavior, compared to the change in Q. As seen, the detonation is always unstable at $10 < Q < 40$ under the selected ϕ range. The trend of the neutral curves agrees with the discussion in Subsection IV D that ϕ plays a minor role in the detonation stability when vibrational nonequilibrium is significant.

The features found in the neutral stability curves confirm with the short summaries made in the previous subsections. That is, the detonation is stabilized when vibrational relaxation is introduced in the chemical kinetics, and the instability region occupied in the neutral stability curves are shrunk clearly. At the limit $Q \to 0$, the detonation is always inert to the perturbation, and this condition has also been reported in the literature.[15,56] Since the change in the

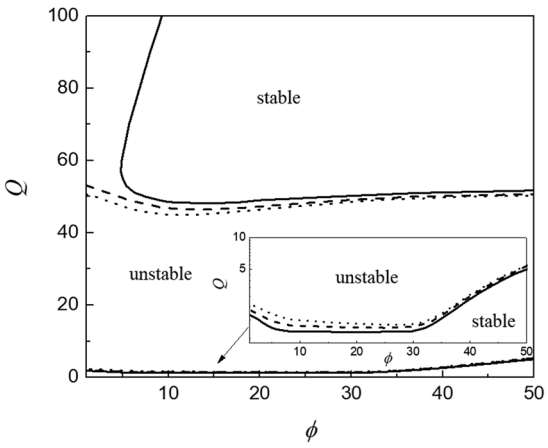

FIG. 12. The neutral stability curve with Q vs ϕ at $\tau^{c/v}$ = 3 (dotted), $\tau^{c/v}$ = 7 (dashed), and $\tau^{c/v}$ = 700 (solid). γ = 1.2, f = 1, and E_a = 26.

Published under license by AIP Publishing

value of Q would solely affect the chemical reaction rate evaluated in the Arrhenius model [i.e., Eq. (4)], it provides an insight that the stabilization effect by vibrational relaxation (shift of the neutral stability boundary in E_a and f) always exists regardless of the chemical reaction rate.

F. Comparison with stability analysis results computed by numerical scheme

Many studies have revealed that both the neutral stability limits and the corresponding frequencies predicted in LSA match those computed in numerical simulation near the stability boundary.[16] To justify the LSA findings in this study, simulation is conducted in selected cases for which the neutral stability limits and periods of oscillation between the two approaches are compared. Notably, Subsections IV B–IV D have demonstrated an extreme case of very high $\tau^{c/v}$ (i.e., $\tau^{c/v} = 700$) representing the state of thermal equilibrium with the predicted neutral stability limit, and these are also verified in this section.

Table II shows a comparison of the neutral stability limit and the period of oscillation obtained from both the analytical and numerical approaches for the selected eight cases with $\gamma = 1.2$, $Q = 50$, and $\phi = 20$. The E_a at the neutral stability limit for the first four cases are under the thermal equilibrium state (i.e., case I) and under the thermal nonequilibrium state for $\tau^{c/v} = 5$ (i.e., case II), $\tau^{c/v} = 7$ (i.e., case III), and $\tau^{c/v} = 9$ (i.e., case IV), whereas the other four present the variations of f at the neutral stability limit under the thermal equilibrium state (i.e., case V) and under the thermal nonequilibrium state for $\tau^{c/v} = 5$ (i.e., case VI), $\tau^{c/v} = 10$ (i.e., case VII), and $\tau^{c/v} = 20$ (i.e., case VIII). Notably, to construct the thermal equilibrium simulation, the vibrational relaxation mechanism, i.e., Eq. (6), was neglected in the chemical kinetics, while the vibrational energy term, i.e., Eq. (3), was calculated with $T_v = T_{tr}$. A similar treatment has been conducted in the numerical simulation of one-dimensional hydrogen–oxygen detonation diluted with argon.[30] For reference, a shock pressure history of the case with $E_a = 26.47$ under the thermal equilibrium state is presented in Fig. 13, representing the neutral stability limit for case I. The period of oscillation is then identified by averaging the period between peak amplitudes and is calculated to be 10.64. Note that the initial damping in Fig. 13 is due to the numerical startup error, and a stable configuration is achieved after a long-time evolution.[22]

TABLE II. Comparison of the neutral stability limit and the period of oscillation computed by linear stability analysis and numerical simulation, respectively. $\gamma = 1.2$, $Q = 50$, and $\phi = 20$. NSL—Neutral stability limit and PO—period of oscillation. Case I: $f = 1$ is fixed at thermal equilibrium. Case II: $f = 1$ is fixed at thermal nonequilibrium with $\tau^{c/v} = 5$. Case III: $f = 1$ is fixed at thermal nonequilibrium with $\tau^{c/v} = 7$. Case IV: $f = 1$ is fixed at thermal nonequilibrium with $\tau^{c/v} = 9$. Case V: $E_a = 50$ is fixed at thermal equilibrium. Case VI: $E_a = 50$ is fixed at thermal nonequilibrium with $\tau^{c/v} = 5$. Case VII: $E_a = 50$ is fixed at thermal nonequilibrium with $\tau^{c/v} = 10$. Case VIII: $E_a = 50$ is fixed at thermal nonequilibrium with $\tau^{c/v} = 20$.

	Linear stability analysis		Numerical simulation	
Case	NSL	PO	NSL	PO
I	$E_a = 26.46$	10.63	$E_a = 26.47$	10.64
II	$E_a = 27.13$	12.14	$E_a = 27.14$	12.15
III	$E_a = 26.99$	11.77	$E_a = 27.02$	11.74
IV	$E_a = 26.90$	11.54	$E_a = 26.92$	11.51
V	$f = 1.62$	8.02	$f = 1.62$	8.03
VI	$f = 1.555$	9.51	$f = 1.554$	9.52
VII	$f = 1.582$	8.80	$f = 1.581$	8.83
VIII	$f = 1.60$	8.46	$f = 1.598$	8.43

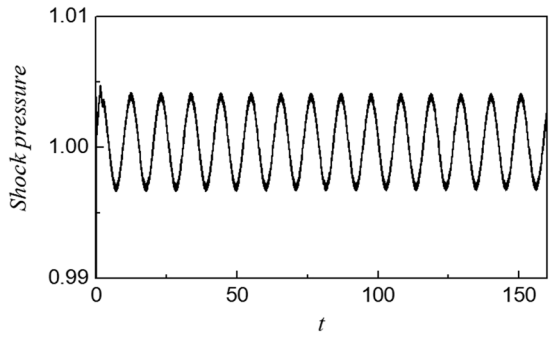

FIG. 13. Shock pressure history at $E_a = 26.47$ under the thermal equilibrium state computed by numerical simulation. $\gamma = 1.2$, $Q = 50$, $\phi = 20$, and $f = 1$.

Regarding the LSA result subjected to the changes in E_a and f, the cases with $\tau^{c/v} = 700$ denoting the thermal equilibrium state are presented in cases I and V for comparison, while the cases with $\tau^{c/v} = 5$, 7, 9, 10, and 20 are presented in other cases denoting the state of thermal nonequilibrium. The period of oscillation PO in LSA can be calculated through the following expression:

$$\mathrm{PO} = \frac{2\pi}{\mathrm{Im}(\alpha)}, \tag{30}$$

where $\mathrm{Im}(\alpha)$ is on the Erpenbeck scale for easy demonstration. Note that the discussion of different scales in LSA has been presented in Subsection IV A above. The conversion factors to the Erpenbeck scale in this study are 2.403, 2.886, 2.907, 2.921, and 2.937 for $f = 1$, 1.555, 1.582, 1.60, and 1.62, respectively. For instance, $\mathrm{Im}(\alpha)$ obtained in case I at $E_a = 26.46$ is 0.245, and the period of oscillation can then be evaluated by $2\pi/(0.246 \times 2.403)$ equal to 10.63.

As shown in Table II, the data from the two approaches matched closely with each other, and the difference is at most 0.03. Hence, the discussion in LSA is well validated in this study considering vibrational–chemical coupling chemistry.

V. CONCLUSIONS

A linear stability analysis of one-dimensional detonation with a vibrational–chemical coupling mechanism is investigated using the normal mode approach. With the introduction of the time ratio $\tau^{c/v}$ denoting the chemical reaction time scale vs the vibrational relaxation time scale, the chemical kinetics are constructed such that an Arrhenius reaction rate is coupled with the vibrational relaxation rate using Park's averaged two-temperature model. The activation energy E_a in the Arrhenius model, the degree of overdrive f, the heat release Q, and the characteristic vibrational temperature ϕ are chosen for a parametric study with $\gamma = 1.2$ kept constant.

Published under license by AIP Publishing

On the change in E_a with different $\tau^{c/v}$, it is shown that both the fundamental mode and the first overtone are observed in the analysis. The appearance of the first overtone may be attributed to the multi-chemical kinetics involved in the reaction model, analogous to the LSA findings of pathological detonation in the literature. When $\tau^{c/v}$ decreases, shifts of the neutral stability limit and the bifurcation point (with a corresponding lower growth rate) to a higher E_a are observed. This finding implies that the detonation is stabilized under vibrational or thermal nonequilibrium. Through the analysis of the ratio of induction length to the exothermic reaction length at different $\tau^{c/v}$, the stabilization effect due to vibrational relaxation is explained. On the other hand, neither the neutral stability limit nor the bifurcation point would be shifted in the stability spectrum when $\tau^{c/v} \geq 275$, and this critical condition reveals that the detonation is under the state of thermal equilibrium. The vibrational time scale is sufficiently small compared with the chemical time scale at this stage, and equilibrium is quickly established immediately after the start of the reaction. The corresponding neutral stability limit is at $E_a = 26.46$.

For detonations with different degrees of overdrive f, both the fundamental mode and the first overtone are demonstrated in the analysis again. As reported in the previous literature, an increase in f would stabilize the detonation, and thus, a neutral stability limit should be obtained at $f > 1$. By decreasing $\tau^{c/v}$, the neutral stability limit shifts to the lower f accordingly. Since both the increase in f and the decrease in $\tau^{c/v}$ provide the stabilization effect in detonation propagation, the introduction of vibrational relaxation in the analysis contributed to the shift of both the stability limit and the bifurcation point. The critical $\tau^{c/v}$ above which the detonation is at thermal equilibrium is at $\tau^{c/v} = 252$, and the corresponding neutral stability limit is at $f = 1.62$.

Regarding the sensitivity study to the change in ϕ, two test conditions are implemented in the analysis—one has a single unstable oscillatory eigenmode and the other has two unstable nonoscillatory eigenmodes. For the case with a single unstable mode, a minimum growth rate is found at approximately $\phi = 10$ for all selected $\tau^{c/v}$, and a shift of the stability spectrum to a lower growth rate with decreasing $\tau^{c/v}$ is again observed. Similarly, a shift of the upper eigenmode to the lower level with decreasing $\tau^{c/v}$ is manifested clearly in the other tested case, but little effect on the shift of the lower eigenmode is shown under the change in ϕ. Overall, ϕ shows little effect on stabilizing the detonation compared with that of the variation in E_a and f, and no change in the number of eigenmodes is observed throughout the selected ϕ ranges.

To examine the change in instability regimes at different heat release Q, neutral stability curves of Q–E_a, Q–f, and Q–ϕ are presented as $\tau^{c/v}$ varies. Among all the curves, the instability regions become smaller accordingly when $\tau^{c/v}$ decreases, confirming that the detonation is stabilized under the significant vibrational nonequilibrium. In addition, another Q–E_a curves with different γ are presented under the vibrational equilibrium/nonequilibrium state. The stabilization effect is always observed regardless of the choice of γ. The change in the value of Q would affect the chemical reaction rate evaluated in the Arrhenius model only, while the stabilization effect by vibrational relaxation remains.

To justify the normal mode result from LSA, numerical simulation is conducted on selected cases to see if the neutral stability limit and the period of oscillation computed match with that from the analytical approach. A conversion between the Erpenbeck scale and the scale utilized in this study is necessary for easy demonstration. As shown, the difference between the two results is at most 0.03 in either the neutral stability limit or the period of oscillation. Therefore, the analysis of vibrational–chemical coupling kinetics in this report is well validated.

ACKNOWLEDGMENTS

The authors thank the Hong Kong Research Grants Council (Grant No. 152065/19E) and the National Natural Science Foundation of China (Grant No. 11772284) for financial support.

DATA AVAILABILITY

The data that support the findings of this study are available within the article.

REFERENCES

[1]Y. B. Zeldovich, "On the theory of the propagation of detonation in gaseous systems," Zh. Exp. Teor. Fiz. **10**(5), 542 (1940) [English translation, NACA TN No. 1261 (1950)].
[2]J. von Neumann, Theory of detonation waves, O.S.R.D. Report 549 (1942).
[3]W. Döring, "On detonation processes in gases," Ann. Phys. **43**, 9 (1943).
[4]W. Fickett and W. C. Davis, *Detonation* (University of California Press, 1979).
[5]Y. Zhang, L. Zhou, J. Gong, H. D. Ng, and H. Teng, "Effects of activation energy on the instability of oblique detonation surfaces with a one-step chemistry model," Phys. Fluids **30**, 106110 (2018).
[6]P. Yang, H. D. Ng, H. Teng, and Z. Jiang, "Initiation structure of oblique detonation waves behind conical shocks," Phys. Fluids **29**, 086104 (2017).
[7]G. X. Xiang, X. Gao, W. J. Tang, X. Z. Jie, and X. Huang, "Numerical study on transition structures of oblique detonations with expansion wave from finite-length cowl," Phys. Fluids **32**, 056108 (2020).
[8]Y. Liu, W. Zhou, Y. Yang, Z. Liu, and J. Wang, "Numerical study on the instabilities in H_2-air rotating detonation engines," Phys. Fluids **30**, 046106 (2018).
[9]D. S. Stewart and A. R. Kasimov, "State of detonation stability theory and its application to propulsion," J. Propul. Power **22**, 1230 (2006).
[10]J. J. Erpenbeck, "Stability of steady-state equilibrium detonations," Phys. Fluids **5**, 604 (1962).
[11]J. J. Erpenbeck, "Structure and stability of the square-wave detonation," Symp. (Int.) Combust. **9**, 442 (1963).
[12]J. J. Erpenbeck, "Stability of idealized one-reaction detonations," Phys. Fluids **7**, 684 (1964).
[13]H. I. Lee and D. S. Stewart, "Calculation of linear detonation instability: One-dimensional instability of plane detonation," J. Fluid Mech. **216**, 103 (1990).
[14]G. J. Sharpe, "Linear stability of idealized detonations," Proc. R. Soc. London, Ser. A **453**, 2603 (1997).
[15]M. Short and D. S. Stewart, "Cellular detonation stability. Part 1. A normal-mode linear analysis," J. Fluid Mech. **368**, 229 (1998).
[16]G. J. Sharpe, "Linear stability of pathological detonations," J. Fluid Mech. **401**, 311 (1999).
[17]A. R. Kasimov and D. S. Stewart, "Spinning instability of gaseous detonations," J. Fluid Mech. **466**, 179 (2002).
[18]S. D. Watt and G. J. Sharpe, "One-dimensional linear stability of curved detonations," Proc. R. Soc. London, Ser. A **460**, 2551 (2004).
[19]G. J. Sharpe and S. A. E. G. Falle, "Numerical simulations of pulsating detonations: I. Nonlinear stability of steady detonations," Combust. Theory Modell. **4**, 557 (2000).
[20]M. Short and J. J. Quirk, "On the nonlinear stability and detonability limit of a detonation wave for a model three-step chain-branching reaction," J. Fluid Mech. **339**, 89 (1997).

Published under license by AIP Publishing

[21] J. H. Lee, *The Detonation Phenomenon* (Cambridge University Press Cambridge, 2008).
[22] H. D. Ng, M. I. Radulescu, A. J. Higgins, N. Nikiforakis, and J. H. S. Lee, "Numerical investigation of the instability for one-dimensional Chapman-Jouguet detonations with chain-branching kinetics," Combust. Theory Modell. **9**, 385 (2005).
[23] M. Short and G. Sharpe, "Pulsating instability of detonations with a two-step chain-branching reaction model: Theory and numerics," Combust. Theory Modell. **7**, 401 (2003).
[24] G. J. Sharpe, "Numerical simulations of pulsating detonations: II. Piston initiated detonations," Combust. Theory Modell. **5**, 623 (2001).
[25] L. He and J. H. S. Lee, "The dynamical limit of one-dimensional detonations," Phys. Fluids **7**, 1151 (1995).
[26] G. J. Sharpe and S. A. E. G. Falle, "One-dimensional numerical simulations of idealized detonations," Proc. R. Soc. London, Ser. A **455**, 1203 (1999).
[27] S. D. Watt and G. J. Sharpe, "Linear and nonlinear dynamics of cylindrically and spherically expanding detonation waves," J. Fluid Mech. **522**, 329 (2005).
[28] B. D. Taylor, A. R. Kasimov, and D. S. Stewart, "Mode selection in weakly unstable two-dimensional detonations," Combust. Theory Modell. **13**, 973 (2009).
[29] B. Taylor, D. Kessler, and E. Oran, *Estimates of Vibrational Nonequilibrium Time Scales in Hydrogen-Air Detonation Waves* (Taipei, Taiwan, 2013).
[30] L. Shi, H. Shen, P. Zhang, D. Zhang, and C. Wen, "Assessment of vibrational non-equilibrium effect on detonation cell size," Combust. Sci. Technol. **189**, 841 (2016).
[31] R. Fiévet, S. Voelkel, H. Koo, V. Raman, and P. L. Varghese, "Effect of thermal nonequilibrium on ignition in scramjet combustors," Proc. Combust. Inst. **36**, 2901 (2017).
[32] S. Voelkel, D. Masselot, P. L. Varghese, and V. Raman, "Analysis of hydrogen-air detonation waves with vibrational nonequilibrium," AIP Conf. Proc. **1786**, 070015 (2016).
[33] H. Koo, V. Raman, and P. L. Varghese, "Direct numerical simulation of supersonic combustion with thermal nonequilibrium," Proc. Combust. Inst. **35**, 2145 (2015).
[34] K. C. Uy, L. Shi, and C. Wen, "Chemical reaction mechanism related vibrational nonequilibrium effect on the Zel'dovich–von Neumann–Döring (ZND) detonation model," Combust. Flame **196**, 174 (2018).
[35] K. C. K. Uy, L. S. Shi, and C. Y. Wen, "Prediction of half reaction length for H_2O_2Ar detonation with an extended vibrational nonequilibrium Zel'dovich–von Neumann–Döring (ZND) model," Int. J. Hydrogen Energy **44**, 7667 (2019).
[36] W. Han, C. Wang, and C. K. Law, "Pulsation in one-dimensional H_2–O_2 detonation with detailed reaction mechanism," Combust. Flame **200**, 242 (2019).
[37] W. G. Vincenti and C. H. Kruger, *Introduction to Physical Gas Dynamics* (Wiley, New York, 1967).
[38] C. Park, "Assessment of two-temperature kinetic model for ionizing air," J. Thermophys. Heat Transfer **3**, 233 (1989).
[39] S. Voelkel, V. Raman, and P. L. Varghese, "Effect of thermal nonequilibrium on reactions in hydrogen combustion," Shock Waves **26**, 539 (2016).
[40] P. A. Gnoffo, R. N. Gupta, and J. L. Shinn, "Conservation equations and physical models for hypersonic air flows in thermal and chemical nonequilibrium," NASA Technical Paper No. 2867, 1989.
[41] H. He, S.-T. Yu, and Z.-C. Zhang, "Direct calculations of one-, two-, and three-dimensional detonations by the CESE method," in *43rd AIAA Aerospace Sciences Meeting and Exhibit: American Institute of Aeronautics and Astronautics* (AIAA, 2005).
[42] J. D. Buckmaster and G. S. S. Ludford, "The effect of structure on the stability of detonations I. Role of the induction zone," Symp. (Int.) Combust. **21**, 1669 (1988).
[43] S.-C. Chang, "The method of space-time conservation element and solution element—A new approach for solving the Navier-Stokes and Euler equations," J. Comput. Phys. **119**, 295 (1995).
[44] H. Shen, C.-Y. Wen, K. Liu, and D. Zhang, "Robust high-order space-time conservative schemes for solving conservation laws on hybrid meshes," J. Comput. Phys. **281**, 375 (2015).
[45] C. Y. Wen, H. Saldivar Massimi, and H. Shen, "Extension of CE/SE method to non-equilibrium dissociating flows," J. Comput. Phys. **356**, 240 (2018).
[46] H. Shen, C.-Y. Wen, M. Parsani, and C.-W. Shu, "Maximum-principle-satisfying space-time conservation element and solution element scheme applied to compressible multifluids," J. Comput. Phys. **330**, 668 (2017).
[47] H. Shen, C.-Y. Wen, and D.-L. Zhang, "A characteristic space-time conservation element and solution element method for conservation laws," J. Comput. Phys. **288**, 101 (2015).
[48] H. Shen and C.-Y. Wen, "A characteristic space-time conservation element and solution element method for conservation laws II. Multidimensional extension," J. Comput. Phys. **305**, 775 (2016).
[49] E. Fan, B. Guan, C.-Y. Wen, and H. Shen, "Numerical study on the jet formation of simple-geometry heavy gas inhomogeneities," Phys. Fluids **31**, 026103 (2019).
[50] B. Guan, Y. Liu, C.-Y. Wen, and H. Shen, "Numerical study on liquid droplet internal flow under shock impact," AIAA J. **56**, 3382 (2018).
[51] B. Guan, D. Wang, G. Wang, E. Fan, and C.-Y. Wen, "Numerical study of the Richtmyer–Meshkov instability of a three-dimensional minimum-surface featured SF_6/air interface," Phys. Fluids **32**, 024108 (2020).
[52] Y. Liang, Y. Jiang, C.-Y. Wen, and Y. Liu, "Interaction of a planar shock wave and a water droplet embedded with a vapour cavity," J. Fluid Mech. **885**, R6 (2020).
[53] Y. Liang, Z. Zhai, X. Luo, and C.-Y. Wen, "Interfacial instability at a heavy/light interface induced by rarefaction waves," J. Fluid Mech. **885**, A42 (2020).
[54] Z. Zhai, F. Zhang, Z. Zhou, J. Ding, and C.-Y. Wen, "Numerical study on Rayleigh-Taylor effect on cylindrically converging Richtmyer-Meshkov instability," Sci. China: Phys., Mech. Astron. **62**, 124712 (2019).
[55] H. Shen and M. Parsani, "The role of multidimensional instabilities in direct initiation of gaseous detonations in free space," J. Fluid Mech. **813**, R4 (2017).
[56] D. I. Kabanov and A. R. Kasimov, "Linear stability analysis of detonations via numerical computation and dynamic mode decomposition," Phys. Fluids **30**, 036103 (2018).
[57] H. Ng, A. Higgins, C. Kiyanda, M. Radulescu, J. Lee, K. Bates, and N. Nikiforakis, "Nonlinear dynamics and chaos analysis of one-dimensional pulsating detonations," Combust. Theory Modell. **9**, 159 (2005).

Published under license by AIP Publishing